Evaluating single-sided natural ventilation models against full-scale idealised measurements: impact of wind direction and turbulence

Building and Environment 170 (2020) 106556

Contents lists available at ScienceDirect

Building and Environment

journal homepage: http://www.elsevier.com/locate/buildenv

Evaluating single-sided natural ventilation models against full-scale idealised measurements: Impact of wind direction and turbulence

H.L. Gough [a], J.F. Barlow [a,*], Z. Luo [b], M.-F. King [c], C.H. Halios [b], C.S.B. Grimmond [a]

[a] Department of Meteorology, University of Reading, United Kingdom
[b] School of the Built Environment, University of Reading, United Kingdom
[c] School of Civil Engineering, University of Leeds, United Kingdom

ARTICLE INFO

Keywords:
Natural ventilation
Cubes
Wind-driven
Full-scale
Sheltering
Turbulence

ABSTRACT

Commonly single-sided natural ventilation is used in temperate climates to provide comfortable and healthy indoor environments. However, within built-up areas it is difficult to predict natural ventilation rates for buildings as they depend on many flow factors and opening type. Here, existing models are evaluated using the nine-month Refresh Cube Campaign (RCC). Pressure-based ventilation rates were determined for a small opening (1% porosity) in a cubical test building (side = 6 m). The building was isolated and then sheltered in a limited staggered building array to simulate turbulent flows in dense urban areas. Internal and external flow, temperature and pressure measurements captured a wide range of scales of variability. Although the Warren and Parkins (1985, WP85) model performed best for 30-min mean ventilation rates, all four models tested underestimated ventilation rates by a factor of 10. As wind dominated the stack effect, new coefficients were derived for the WP85 wind-driven model as a function of wind angle. Predictions were mostly improved, except for directions with complex flow patterns during the sheltered case. For the first time, the relation between ventilation rate and turbulence intensity (TI) around a full-scale building was tested. Results indicate that the wind-driven model for single-sided ventilation in highly turbulent flows ($0.5 < TI < 4$) can be improved by including TI as a multiplicative factor. Although small window openings with highly turbulent flows are common for sheltered buildings in urban areas, future model development should include a variety of configurations to assess the generality of these results.

1. Introduction

Natural ventilation is an important passive building design strategy for the development of sustainable and healthy indoor environments [1–4]. Whilst cross ventilation is often preferred for its larger flow rates, few buildings can achieve cross-ventilation fully due to the interior partitions, obstacles, and thicknesses [5], and single-sided ventilation is more commonly used [6–9]. Accurate prediction of single-sided ventilation is required; otherwise if ventilation rates are overestimated buildings may overheat and lead to a general distrust of the effectiveness of natural ventilation [10].

Single-sided ventilation of buildings, especially in built-up areas, is difficult to predict as it depends on many factors: wind speed, external-internal temperature difference, indoor temperature gradients, wind direction, turbulence, location, surroundings and type of opening. All or some of these may be accounted for depending on model complexity and the data used in model development. Generally, there is a lack of long-term, comprehensive full-scale data to evaluate these models.

This study focuses on evaluating a series of empirical single-sided ventilation models using observations from the Refresh Cube Campaign (RCC) [23]. Nine months of ventilation and meteorological data were taken around and inside a simple, 6 m tall test building located in a rural setting in the UK. Pressure-based, single-sided ventilation rates were determined for a small opening when the building was both isolated and sheltered within a limited, simplified, staggered building array to characterise turbulent flows in dense urban areas. Discrepancies between the models and observations are interpreted in light of directional effects on wind-speed and turbulence. Uniquely in this study (1) data for a building in both an isolated and a simple array are analysed; and (2) the meteorological and upstream aerodynamic roughness characteristics of the site are very well characterised.

* Corresponding author. Department of Meteorology, University of Reading, Earley Gate, PO Box 243, Reading, RG6 6BB, UK.
E-mail address: j.f.barlow@reading.ac.uk (J.F. Barlow).

https://doi.org/10.1016/j.buildenv.2019.106556
Received 16 August 2019; Received in revised form 21 October 2019; Accepted 15 November 2019
Available online 19 November 2019

2. Existing empirical expressions to calculate single-sided natural ventilation

Chen [11] reviews the methodology used for assessing ventilation model performance and recent applications. There are several empirical expressions for the calculation of single-sided natural ventilation. Four empirical expressions derived from wind tunnel or full-scale measurement (Table 1) can be directly compared to our full-scale measurement dataset. Each equation has either a wind-driven or a buoyancy-driven component, or a combination of the two. Equations developed from CFD simulations (e.g. [5]) cannot be assessed as not all input variables have been measured and thus are only discussed briefly.

Generally, calculation of the thermally driven component of ventilation (Q_{stack}) uses Warren and Parkin's (WP85) equation [12] (Table 1) [12,13]. offered two ways to calculate the wind driven ventilation component (Q_{wind}) depending if local (U_{local}) or reference (U_{ref}) wind speed measurements are available (Table 1). "Local" is taken to refer to measurement closest to the opening. The methods to calculate A_{eff} depend on opening layout. The total ventilation rate (Q) is determined to be the largest of Q_{wind} and Q_{stack} [13]. However, this does not consider interactions between Q_{wind} and Q_{stack}. These may reinforce or counter the effects of each other, depending on external conditions. The empirical equations are derived from both wind tunnel and full-scale data [12]. As these empirical expressions for single-sided natural ventilation are often only tested with the original data, their general applicability is unknown. Exceptions to this include [14–16] who compare their data to pre-existing models such as [12,17,18] and suggest improvements to the pre-existing models.

De Gids and Phaff's (1982) (DP82) [17] equation, derived from full-scale measurements at 33 buildings (Table 1), considers both thermal and wind driven components. For the three urban locations, surrounding buildings were up to four floors high. All measurements were undertaken on the first floor of the test buildings with wind speeds, window and room air velocities, air change rates, opening area and temperature measured [17]. This work is used in both the French Thermal Regulation of buildings and the European standard to predict the impact of window opening in buildings [19]. U_{ref} is measured at 10 m. Unlike WP85, C_D (discharge coefficient) is not explicitly used within DP82 but is within a square root term with dimensions of velocity [14]. This means the accuracy is dependent on the opening type. Using the pre-multiplying factor of 0.5 assumes only half a single-sided opening is acting as an inlet at any given time [17]. acknowledged it is difficult to define the velocity profile shape in the opening, as this depends on the dominant process (i.e. buoyancy or wind).

The standard EN 16798-7:2017 [20] (Table 1) improved DP82 using the changes discussed in Ref. [10]. Notably, like [12], it uses the maximum of wind and thermally-driven ventilation rate terms. Given the risk of overestimation of ventilation rate [10], the constant turbulence term (C_3, Table 1) is removed.

Larsen and Heiselberg (2008) (LH08) [14] used the same basic form as [17] with three coefficients (C_{L1}, C_{L2}, C_{L3}) derived using least squares regression with wind-tunnel data. Data were grouped into leeward, windward or parallel wind directions (Table 1) and compared to the results. They assumed that $f(\beta_v)\sqrt{C_p}$ (a function of wind direction, β_v and pressure coefficient, C_p) is equivalent to the ratio of local to reference wind speeds. The coefficients and functions are derived from 159 wind tunnel cases, spanning a range of wind speeds (0, 3 and 5 m s^{-1}), wind directions (β_v = 0°–345°) and temperature differences (ΔT = 0, 5 and 10 °C).

Caciolo et al. (2011) [15] varied the opening type using openings that were plain, top hung and bottom hung, with the latter two having both 12° and 28° opening angles. They compared the results of [12,14,18] to data for a second floor full scale room exposed to natural conditions [15]. found WP85 yielded the best results (accuracy ± 25%) but all provided reasonably good correlations. A similar model accuracy was found by Ref. [10] for WP85, who also found that LH08 underestimated wind tunnel measurements. Zhou et al. [8] found that LH08 underestimated their LES-derived ventilation rates, and WP85, DG82 and their own model gave similar results to the data. However, Caciolo et al. (2013) [16] highlighted that the correlations tested ([12,14,18]) did not account for the reduction of airflow rate in leeward conditions. Hence, the model proposed in [16] is designed to be applied to single sided ventilation on the leeward side of a building. WP85 over-predicted the ventilation rate in leeward conditions. This is related to the wind counteracting the stack effect by mixing the air at the opening, reducing the effective temperature difference, with higher winds leading to a greater reduction [16]. The air change rate caused by wind driven effects is not considered in this model (Table 1) [16]. Uses a similar form for Q_{stack} as [12] but includes ΔT^* (ratio of effective temperature difference at the opening to indoor-outdoor temperature difference) for

Table 1
Single-sided ventilation rate equations from the literature, hereafter referred to by the acronyms given in column 1. The data from which models were derived were measured in the wind tunnel (WT) or at full scale (FS). Common terms are defined only once.

Model	Data	Equation	Symbols
Warren and Parkins (1985), Warren (1977) WP85, W77 [12,13]	FS WT	$Q_{Wwind} = 0.025\,A\,U_{ref}Q_{Wwind} = 0.1AU_{local}Q_{stack} = \frac{1}{3}A_{eff}C_D\sqrt{\frac{\Delta T\,H\,g}{T_{av}}}Q_W = \max(Q_{Wwind}; Q_{stack})$	A_{eff} effective opening area U_{ref} reference wind speed U_{local} local wind speed C_D discharge coefficient ΔT temperature difference across the opening H height of the opening (i.e. distance from top to bottom of the opening) T_{av} average of internal and external temperatures g gravitational acceleration
De Gids & Phaff (1982) DP82 [17]	FS	$Q_{PG} = 0.5\,A\sqrt{C_1U_{ref}^2 + C_2H\,\lvert\Delta T\rvert + C_3}$ where $C_1 = 0.001$, $C_2 = 0.0035$ and $C_3 = 0.01$	A opening area C_1 dimensionless coefficient linked to the wind effect C_2 related to the stack effect C_3 related to the turbulence in the oncoming flow
EN 16798-7:2017 EN17 [20]	FS (data from DP82)	$Q_{EN} = \frac{\rho_{int}}{\rho_{ext}}\frac{A}{2}.\max(C_1U_{ref}^2 + C_2H\,\lvert\Delta T\rvert)^{0.5}$ where $C_1 = 0.001$, $C_2 = 0.0035$	ρ_{int} density of internal air ρ_{ext} density of external air
Larsen and Heiselberg (2008) LH08 [14]	WT	$Q_{LH} = A\sqrt{C_{L1}f(\beta_v)^2\lvert C_p\rvert\,U_{ref}^2 + C_{L2}H\,\Delta T + C_{L3}\left(\frac{\Delta C_{p,\,opening}\Delta T}{U_{ref}^2}\right)}$	C_{L1}, C_{L2}, C_{L3} derived using least squares from 159 WT measurements but values not stated by authors β_v Wind direction $\lvert C_p\rvert$ Pressure coefficient $\Delta C_{p,\,opening}$ Difference in pressure coefficients across the opening

leeward conditions, defaulting to WP85 in all other cases (Table 1). However, due to a lack of leeward data in the present study dataset, assessment of the model in [16] is not possible.

Other emprical relations exist (e.g. Dascalaki et al. (1996) [18], Wang and Chen (2012) [21]). As after extensive testing [15] found [18] to systematically overestimate the ventilation rate, we do not evaluate [18]. [21] provides equations for both the mean and the fluctuating ventilation rate components from CFD data. As some of model factors in Ref. [21] (e.g. fluctuating velocity spectrum) are difficult to obtain accurately at full-scale, we do not evaluate [21]. [8]'s modification of [21]'s model showed that the size of the opening could affect the type of flow driving the ventilation. As [8]'s equation requires characteristics not measured in the present study (e.g. position of the neutral plane) we cannot evaluate it.

3. Methodology

As a detailed overview of the site, Refresh Cube Campaign (RCC) and the measurements are provided in [22–26], only the single-sided ventilation data for the model comparison are discussed here. The test building was a 6 m × 6 m x 6 m metal cube [27,28] in rural Silsoe, UK (52.01088° N, −0.410979° W). It had removable openings (0.4 m wide by 1 m high, centre point 3.5 m from the ground) in the front and back faces (Fig. 1). The cube front face was in the prevailing wind direction (~240°), hereafter referred to as 0° (clockwise angles are positive, anticlockwise angles negative, Fig. 1). Hence, 0° denotes flow perpendicular to the front opening (Front or West face: Fig. 1) with ±90° being parallel to the opening.

Fig. 1 shows that the RCC experiment had two spatial arrangements: (1) 'array' (October 2014 to April 2015), and (2) 'isolated' (May 2015 to July 2015). All instruments were kept in the same positions throughout. Following common meteorological practice, we use 30-min means (unless otherwise stated) to capture all the scales of turbulent motion [29] with instruments logged at 10 Hz (except for the "Channel" mast which was logged at 20 Hz).

Seven 3-axis Gill R3-50 sonic anemometers, measuring three-component wind velocity, were deployed within the cube itself (2) and outside (5) (Fig. 1). The centres of the two sonic anemometers closest to the instrumented cube ("Front (Local)" and "Back") and the two internal sonic anemometers were at 3.5 m above ground level (in line with the opening centre). Other sonic anemometers were positioned at heights of 6 m (U_{ref}) and 10 m on the "Reference" mast and at 2.9 m (due to practical limitations) on the "Channel" mast (Fig. 1).

External temperature was measured on the Channel mast using a WXT520 weather station (error at 20 °C = ± 0.3 °C) (Fig. 1). Internal temperature was measured using RS components type-K thermocouples

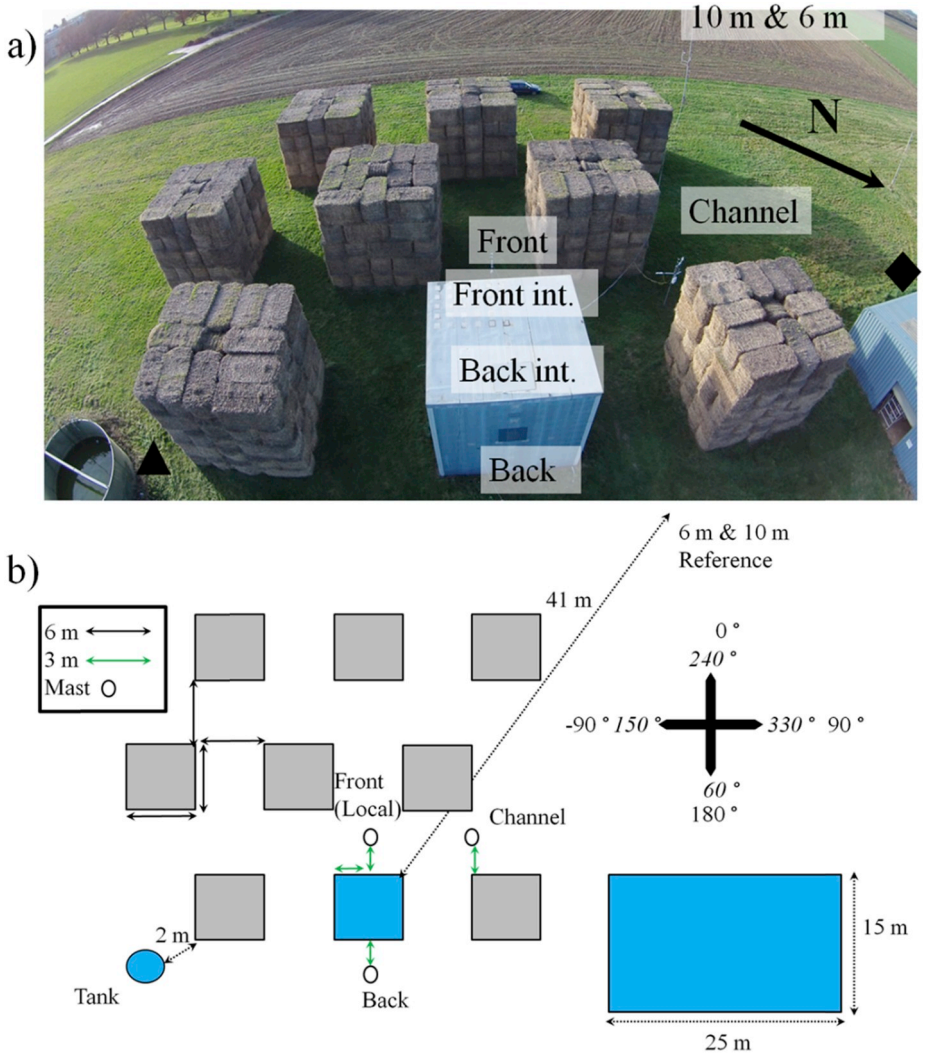

Fig. 1. RCC field site and instrumentation: (a) Aerial image of the cube array facing into the prevailing wind direction with sonic anemometer locations, storage shed (black diamond) and sewage tanks (black triangle) and (b) plan view with measurements and angle notation (bearing in italics). For the isolated case, the grey cubes were removed [23,24].

at 24 points. Temperature measurement details (e.g. locations) are given in [24].

3.1. Pressure measurements

Ventilation rate was determined in two ways, using: (1) pressure measurements across the outside and inside the cube, and (2) tracer gas decay [24]. The 30 external pressure taps (7 mm holes located centrally on 0.6 m^2 steel panels, mounted flush with the cube cladding) were on four faces (Fig. 2): Roof (4), horizontal array on the centre line across the North (4) and South faces (4) and Front (9) and Back faces (9), arranged in vertical (5) and horizontal (4) arrays.

Two internal pressure taps were located under each possible opening (only one used here) to measure the pressure difference across the opening. A reference pressure was measured using a static pressure probe (in house design [30,31]) with a reference dynamic pressure measured using a directional pitot tube (in house) at 6 m (building height) alongside the 6 m reference sonic anemometer (Fig. 1) [24]. provides sensor details.

The external pressure is calculated from the average of the pressure measurements located around the opening: Taps 3, 4, 18 and 19 for the front face and Taps 12, 13, 26 and 27 for the back face (Fig. 2). In all cases, following the work of [32,33], the average of the external taps is calculated before the difference is calculated between external and internal pressures for each 10 Hz reading and a ventilation rate is calculated from Equation (1):

$$Q = C_d A \sqrt{\frac{2|\Delta p|}{\rho}} \tag{1}$$

This instantaneous ventilation rate is then averaged over 30 min (i.e. same period as all the meteorological data). An alternative method is to average the pressure difference over 30 min and then calculate ventilation rate using Equation (1) [24], found a small difference of up to 10% between the two methods for both single sided and cross ventilated measurements.

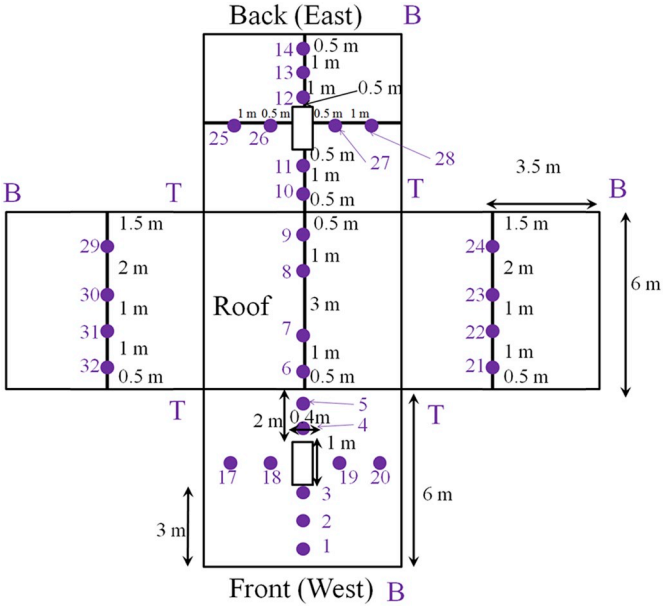

Fig. 2. Location of the pressure taps on each face (T top, B base) of the cube with distance between taps (black) and the opening (white rectangles) [23]. Internal taps 15 and 16 are not shown. (drawing not to scale). Front and back faces are symmetrical as are the side faces.

3.2. Ventilation data overview

Of the 765 single-sided, isolated cube, 30 min measurement periods, 472 contain all the data required to test the empirical models. The remaining 291 have missing temperatures (external or mean internal). For the array case 1104 periods were recorded of which 497 have all the required data. Data were filtered for near-neutral stability (defined using the height of the measurement, Z divided by the Monin-Obukhov length L), where $-0.1 < Z/L < 0.1$ at both the 6 m and 10 m reference masts (Fig. 1), to remove large fluctuations due to atmospheric convection. This reduces the total to 202 isolated and 429 array periods.

Pressure based and tracer gas decay methods of calculating the ventilation rate of the cube are compared in [24] with agreement between the methods being dependent on opening layout and wind direction, with stronger agreement for the single-sided ventilation set-up. A possible explanation for the better agreement relates to when the internal mixing state was less dominated by a single jet (i.e. for oblique wind directions for the isolated case) and generally for the array case where external flows are highly unsteady. There is also the question of the validity of the standard tracer gas decay measurement method in an urban area due to unsteady flows dominating, and choosing the most suitable time-averaging for the measurements. Surrounding buildings may reduce the ability of a building to 'flush' tracer gas out, though this is likely to be dependent on the external building layout [24]. details further the other influencing factors in experimental design.

Only the pressure derived ventilation rates are used here given the relatively few (~100) tracer gas releases available. It should be noted that pressure derived ventilation measurements do not include the effects of infiltration (but steps were taken to minimise infiltration through cracks at the bottom of the cube [23]). Unlike work on pressure coefficients by [30,34] the pressure based ventilation rates are not limited by wind speed, although data are split into three categories: $U_{ref} < 3$ m s^{-1}, $3 < U_{ref} < 6$ m s^{-1} and $U_{ref} > 6$ m s^{-1}.

4. Model performance tested against RCC data

RCC data are tested against a simple model to determine the importance of the stack effect prior to evaluating the models (section 4.2).

4.1. Driving forces of the flow

To determine whether a flow is being driven by buoyant processes (stack effect) or external processes (e.g. wind driven) we use the ratio of external forces to internal viscous forces or Archimedes number (*Ar*):

$$Ar = \frac{g\,\Delta T\,H}{T_{av}U^2} \tag{2}$$

where g is gravitational acceleration, ΔT is the internal to external temperature difference (internal temperature calculated as the average of the 24 indoor sensors), H is the height of the opening (distance from top to the bottom of the opening), T_{av} is the average of internal and external temperatures, and U is the characteristic wind speed, in this case U_{ref}.

A large *Ar* indicates that stack effects dominate while a small *Ar* indicates that wind driven effects dominate. Following a similar method to Warren (1977), Warren and Parkins (1985) and Caciolo et al. (2013), a normalised ventilation rate (or flow number, *F*) is defined:

$$F_{ref} = \frac{Q}{U_{ref}A} \tag{3}$$

where Q (m^3 s^{-1}) is the measured ventilation rate and A (m^2) is the area of the opening. In the following section the reference wind speed (U_{ref}) at 6 m height is used. Based on the flow number (equation (3)), the Archimedes number (equation (2)) and assuming a discharge coefficient

of 0.6, the airflow rate due to the stack effect only is given by [12,16]:

$$F = 0.2\sqrt{Ar} \quad (4)$$

When Equation (4) is plotted, for points close to the line, ventilation results are mostly driven by the stack effect. Above the line, the normalised ventilation rate is higher than that caused by the stack effect alone due to wind driven ventilation reinforcing the stack effect, and below the line the normalised ventilation rate is below that predicted with the stack effect only, suggesting that the wind driven component is acting against the thermal effects.

For the ventilation rates measured in this study, the wind driven ventilation reinforces the stack effect in most 30 min periods in both the isolated and array cases (Fig. 3). Few points lie 'close' (undefined numerically in previous work, e.g. Ref. [15]) to the line for both cases. The flow number values obtained are approximately 10 times larger than prior full-scale buildings studies (cf [11–13]). However [32], reports F ≈ 0.7 for their study using the same isolated cube on the Silsoe site and [21] also has similar flow numbers. The error on ventilation rates is estimated to be up to 15% of the pressure-based ventilation rate, meaning other factors play a role in explaining the spread in observed values.

Our reference mast is within 50 m of the RCC cube in an open rural setting (Fig. 1) whereas the location of the reference mast used by [15,16] is unclear in the more complex site (i.e. low-rise buildings with trees). Thus, their local test building wind speeds may be sheltered compared to the present study, thus reducing their flow numbers. The larger range in wind direction measured during the RCC study increases the spread in results.

Another consideration is the ventilation measurement method used. For single-sided ventilation, the pressure derived ventilation rate has been observed to be around twice the magnitude of the tracer gas decay rate, especially in windward conditions ([24]), leading to larger flow numbers. [15,16] use tracer gas decay. The combination of a larger room in the RCC cube (RCC: 216 m^3 , [15,16]. 27 m^3) and smaller opening (RCC 0.4 m^2 [15,16]: 1 m^2) leads to a difference in wall porosity (RCC 1%, [15,16]; 2%). Such differences may lead to different unsteady ventilation mechanisms (e.g. pulsation) making a larger contribution [19,32], which might explain differences in overall ventilation rates.

4.2. Performance of different ventilation models

Four models (Table 1) (Warren and Parkins (WP85), Larsen and Heiselberg (LH08), De Gids and Phaff (DP82) and EN 16798-7:2017 (EN17)) are evaluated using measured ventilation rates (Q) (Table 2, Fig. 4). For WP85, the local wind speed (U_{local}) used is measured in front of the cube (Front (Local) mast, Fig. 1). LH08 requires C_{L1}-C_{L3} (Table 1) to be determined from standard pressure coefficients for an exposed 2:1 building. Instead, the RCC pressure coefficients and pressure differences measured for both the isolated and array cases are used. Wind angles from the four models are converted to the RCC co-ordinate system (Fig. 1) to ease comparison.

For most of the data Q_{wind} is larger than Q_{stack}. When U_{ref} is used with WP85 for the isolated cube 66 of 202 periods had calculated Q_{stack} larger than Q_{wind}: 56 when U_{ref} was low and 10 medium. When using U_{local}, $Q_{stack} > Q_{wind}$ in only 3 cases, all with low U_{ref}. Using U_{ref} with the WP85 model for the array dataset (429 cases), in 12 (10 low and 2 medium U_{ref}) instances Q_{stack} was larger and 10 (9 low U_{ref} and 1 medium) when using U_{local}. These differences are caused by the array campaign occurring in winter whereas the isolated cube measurements continued into spring/summer.

For WP85-U_{ref} there is an underestimation of the ventilation rate by factor of 10–20 in the isolated case (Figs. 4a) and 10 to 15 in the array case (Fig. 4b). However, ventilation rates are proportional to the observed values and R^2 values are reasonable (Table 2). Despite WP85 being derived from full-scale measurements, this result suggests that the coefficients may not be generally applicable to other full-scale sites.

Using WP85-U_{local} improves the ventilation rate estimates, albeit still a factor of 10 too low (Fig. 4c and d and Table 2). For both the isolated

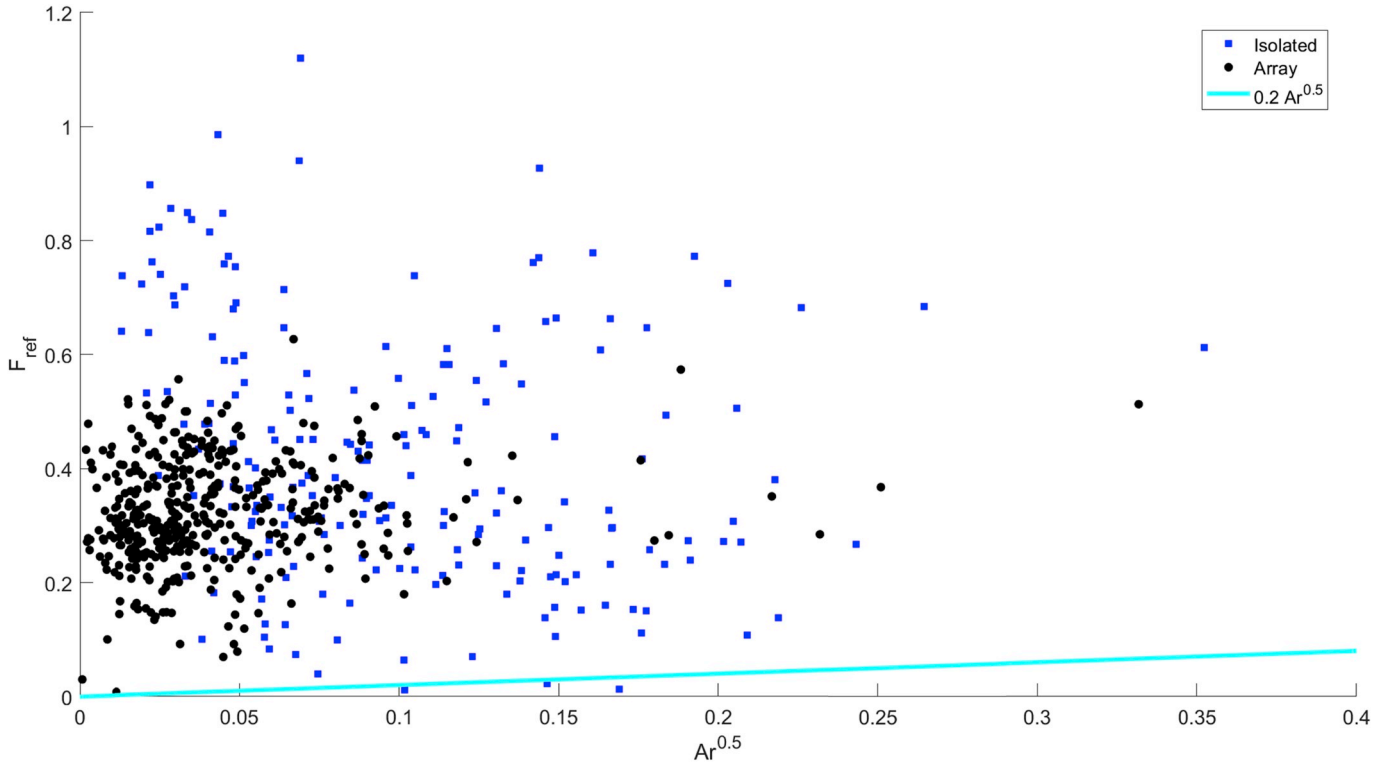

Fig. 3. Flow number (equation (3)) against square root of Archimedes number for the isolated (blue square) and array cases (black circle). Cyan line shows equation (4), $F = 0.2\sqrt{Ar}$. (For interpretation of the references to colour in this figure legend, the reader is referred to the Web version of this article.)

Table 2
Ventilation rate model performance metrics for the (a) isolated cube and (b) array. RMSE (Root Mean Square Error), SE (Standard Error), MAE (Mean Absolute error) MBE (Mean Bias Error).

Model	Gradient	offset	R^2	SE of slope ($m^3\ s^{-1}$)	SE offset ($m^3\ s^{-1}$)	RMSE ($m^3\ s^{-1}$)	MAE ($m^3\ s^{-1}$)	MBE ($m^3\ s^{-1}$)
Isolated								
WP85 U_{ref}	0.027	0.016	0.53	0.0012	0.00078	0.010	0.50	−0.50
WP85 U_{local}	0.010	0.026	0.53	0.0049	0.0036	0.039	0.45	−0.59
DP82	0.0080	0.096	0.02	0.0050	0.0033	0.026	0.50	−1.16
LH08	0.020	0.04	0.08	0.64	0.0051	0.024	0.48	−1.76
EN17	0.121	0.017	0.17	0.0019	0.0098	0.0097	0.51	−1.20
Array								
WP85 U_{ref}	0.055	0.01	0.61	0.0015	0.00094	0.012	0.45	−0.45
WP85 U_{local}	0.056	0.02	0.29	0.0029	0.0016	0.023	0.44	−0.44
DP82	0.061	0.06	0.34	0.0041	0.0063	0.022	0.40	−0.84
LH08	0.018	0.02	0.03	0.0028	0.0027	0.0097	0.47	−1.33
EN17	0.025	0.02	0.32	0.0017	0.0011	0.0092	0.46	−0.97

and array cases, data are split into linear clusters that correlate broadly with wind direction. The array case has three clusters (Fig. 4d) [23]. reported multiple flow behaviours at the local sonic anemometer for the same reference wind direction (e.g. $\theta_{ref} = 180°$), suggesting that the influence of nearby building wakes was a bistable flow process. This could cause lower or higher ventilation rates for the same U_{ref}.

DP82 has similar ventilation rates (Fig. 4e) to WP85 for the isolated cube with a factor of 10–15 underestimation compared to measured values. Coefficients in these models were both based on full-scale data, however it is hard to compare the settings of either building due to little information being given about the surroundings. Indeed, DP82 predicts larger values for the array (Fig. 4f) than the isolated case despite measured values being lower due to sheltering (especially for wind directions near 0°) [23]. For DP82 the non-zero minima are due to the constant C_3 turbulence term. In reality this term should scale with wind speed and account for local buildings' turbulent wakes. EN17 model (Fig. 4i and j) lacks this constant but the resulting performance is quite different: less scatter (R^2 increased) but increased underestimation (larger MBE).

As the LH08 model requires more data (e.g. temperature measurements) there are fewer results due to gaps in the RCC dataset (Fig. 4g and h) but similar magnitudes to the other models are predicted, despite it being the only one derived from wind tunnel data alone. To take into account the differing geometry of the LH08 wind tunnel model and the present cube array, RCC data were used to derive $f(\beta_v)$ (Table 1), following the method of [1]. Despite this the data are clustered according to wind direction.

Overall, all models, regardless of what type of data the empirical formulae have been derived from, underestimate the ventilation rates of both the isolated and array cubes (Table 3). The array caused a decrease in ventilation rate, most marked (50–90%) for near-perpendicular wind directions [23], but WP85-U_{ref} and DP82 actually predict higher values for the array case for these directions. All relations between measured and modelled values demonstrate considerable scatter (Fig. 4). With some clustering of datapoints suggesting that linear regression through the data is inappropriate, this suggests that some models do not capture the complex local flow behaviour observed. Overall, the WP85 model provided the best prediction of measured ventilation rate in agreement with [15], albeit underestimated (MBE = −0.50 for WP85-U_{ref} and −0.59 for WP85-U_{local}).

5. Directional effects on flow and ventilation

Discrepancies between the models and RCC data are explored with respect to directional effects on flow, turbulence and ventilation.

5.1. New WP85 coefficients that vary with wind direction relative to the opening

WP85 performs better than the more complex models whose coefficients may be site- or method-specific. However, WP85's large underestimation suggests that its coefficients are inappropriate for the Silsoe site. The RCC single-sided ventilation data are used to constrain

$$Q_w = C\ A\ U \tag{5}$$

where U is either local or reference wind speed, to derive new directionally dependent coefficients C_{loc} and C_{ref} for both the isolated and array cases. The coefficients are identical to flow numbers, or normalised ventilation rates [12]. With the variation in local wind speed and direction compared to θ_{ref}, the data are stratified into 30° bins using θ_{local}. Bins of 30° are a compromise between variability in ventilation rate with wind direction and data availability (>5 samples per bin) to produce meaningful statistics. For a given $\theta_{ref,}$ at this site θ_{local} can vary if wake or channelled flow from surrounding buildings dominates [23,23]. Hence θ_{local} is chosen as being more representative of the flow direction adjacent to the opening than θ_{ref}. Data are unavailable for some infrequent wind direction bins (e.g. isolated cube and leeward flows, see Tables 3 & 4).

Using equation (5), the binned data are used to determine the C_{local} coefficients if U_{local} is used (or C_{ref} for U_{ref}). MAE and MBE are improved for most angles when using U_{ref}, though not for $\theta_{local} = 30$–90° (Table 3) for the isolated cube. Using U_{local} leads to lower MAE and MBE values for the isolated and array cases (Table 4). For the array case R^2 values are generally lower and MAE values are higher using U_{ref}, apart from directions where flow is parallel to the opening, suggesting that U_{local} is more representative of the flow impacting on the cube.

Using the directionally dependent coefficients (Table 3, Table 4) a ventilation rate is estimated for each measurement (Fig. 5). For the isolated case performance is improved (Table 2, Table 5), showing that the modified WP85 model (equation (5)) works well with appropriate coefficients. The improvement is larger using U_{local} rather than U_{ref}. Scatter is reduced for the array case, but directional discrepancies are still present for windward directions using the local wind speed. This may be due to the dual behaviour described by Ref. [23] for $\theta_{local} = -45$ to 45°, i.e. for the same U_{ref}, two values of U_{local} could be observed, depending on whether flow was dominated by a wake or channelling flow. Such "flow switching" behaviour can be a feature of complex urban flows [35].

5.2. Flow parameters as a function of direction

After LH08, it would be expected that flow numbers have a directional dependence, as U_{local}/U_{ref} changes with wind direction. In addition, the local turbulence intensity, σ_u/U_{local}, changes with wind direction, depending on if the flow next to the opening is affected by a wake or not. Fig. 6 presents the flow data for the RCC site.

Fig. 6 shows the ratio U_{local}/U_{ref} for the Silsoe site for the isolated and array cases. Also shown are the measurements of WP85, as used by LH08 to derive directional dependence function $f(\beta_v)$. Fig. 6a shows that for

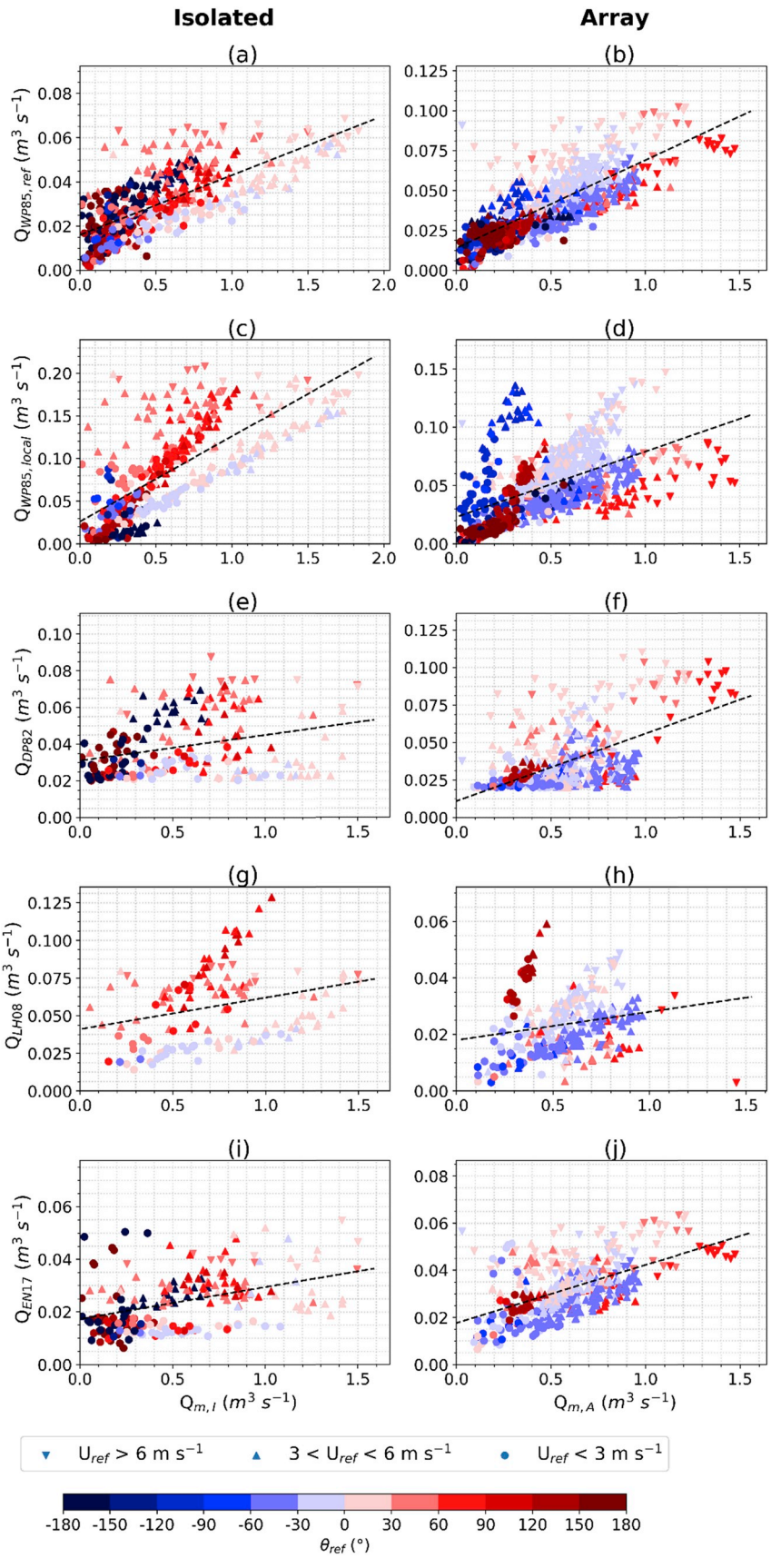

Fig. 4. Modelled and measured ventilation rate, Q, for the isolated (left) and array cases (right). Data is colour coded by wind direction θ_{ref} with the marker shape determined by the magnitude of U_{ref}. Models are labelled as in Table 1: Warren and Parkins (WP85), Larsen and Heiselberg (LH08), EN 16798-7:2017 (EN17) and De Gids and Phaff (DP82), with linear regression lines through all data (Table 2). (For interpretation of the references to colour in this figure legend, the reader is referred to the Web version of this article.)

Table 3
New coefficients for the wind driven WP85 model using U_{ref}. 30° bins based on local wind direction (θ_{local}) used for isolated and array cases. N is the number of data points in each bin and only cases where N > 5 are used. SE is the standard error. Angles equal to the lower bin threshold are placed in the next bin.

θ_{local} range (°)		N	C_{ref}	SE on C_{ref}	R^2	P value	MAE	MBE
Isolated								
−180	*−150*	2	N/A	N/A	N/A	N/A	N/A	N/A
−150	*−120*	0	N/A	N/A	N/A	N/A	N/A	N/A
−120	−90	6	0.198	0.019	0.602	0.001809	0.62	−0.62
−90	*−60*	3	N/A	N/A	N/A	N/A	N/A	N/A
−60	−30	15	0.490	0.025	0.767	2.69E-08	0.23	−0.23
−30	0	14	0.672	0.018	0.940	8.28E-07	0.19	−0.19
0	30	55	0.754	0.012	0.887	1.48E-19	0.33	−0.33
30	60	74	0.562	0.018	0.717	7.56E-27	0.68	−0.68
60	90	74	0.300	0.014	0.403	2.73E-29	1.08	−1.08
90	120	96	0.475	0.010	0.762	1.42E-40	0.60	−0.60
120	150	24	0.298	0.015	0.451	2.13E-09	0.47	−0.47
150	*180*	3	N/A	N/A	N/A	N/A	N/A	N/A
Array								
−180	*−150*	32	0.275	0.014	0.322	7.32E-20	0.78	−0.78
−150	*−120*	7	0.203	0.035	−2.517	0.00086	0.68	−0.68
−120	−90	27	0.225	0.019	0.039	1.62E-11	0.53	−0.53
−90	*−60*	68	0.177	0.006	0.657	1.08E-28	1.02	−1.02
−60	−30	18	0.320	0.013	0.763	1.61E-09	0.87	−0.87
−30	0	33	0.327	0.008	0.897	5.8E-15	0.97	−0.97
0	30	423	0.303	0.005	0.265	4.3E-163	1.35	−1.35
30	60	166	0.305	0.005	0.659	2.62E-80	1.29	−1.29
60	90	6	0.403	0.027	0.945	0.014028	0.85	−0.85
90	120	8	0.320	0.032	0.691	9.68E-05	0.94	−0.94
120	150	90	0.285	0.010	0.360	3.81E-49	0.65	−0.65
150	*180*	28	0.171	0.012	0.058	1.13E-19	0.76	−0.76

Table 4
As Table 3 but using U_{local} with the WP85 model.

θ_{local} range (°)		N	C_{local}	SE on C_{local}	R^2	P value	MAE	MBE
Isolated								
−180	*−150*	2	N/A	N/A	N/A	N/A	N/A	N/A
−150	*−120*	0	N/A	N/A	N/A	N/A	N/A	N/A
−120	−90	6	0.257	0.085	0	0.071651	0.29	−0.29
−90	*−60*	3	N/A	N/A	N/A	N/A	N/A	N/A
−60	−30	15	0.572	0.028	0.845	6.32E-08	0.17	−0.17
−30	0	14	1.089	0.059	0.756	0.00548	0.03	0.03
0	30	55	1.096	0.007	0.983	1.35E-19	0.09	0.09
30	60	74	0.810	0.022	0.796	0.000171	0.19	−0.19
60	90	74	0.376	0.017	0.448	2.74E-25	0.76	−0.76
90	120	96	0.599	0.006	0.938	1.47E-26	0.35	−0.35
120	150	24	1.035	0.046	0.542	0.003092	0.01	0.01
150	*180*	3	N/A	N/A	N/A	N/A	N/A	N/A
Array								
−180	*−150*	32	0.632	0.018	0.789	5.44E-08	0.16	−0.16
−150	*−120*	7	1.478	0.105	0.328	0.000965	0.06	0.06
−120	−90	27	0.530	0.065	−0.707	0.000551	0.12	−0.12
−90	*−60*	68	0.284	0.016	0.227	1.09E-19	0.51	−0.51
−60	−30	18	1.465	0.044	0.873	1.09E-07	0.13	0.13
−30	0	33	1.735	0.025	0.966	6.17E-12	0.20	0.20
0	30	423	0.967	0.020	−0.136	0.00347	0.02	−0.02
30	60	166	0.951	0.021	0.319	0.353715	0.03	−0.03
60	90	6	2.640	0.120	0.979	0.042929	0.36	0.36
90	120	8	0.992	0.177	0.114	0.179533	0.00	0.00
120	150	90	1.016	0.036	0.392	0.000406	0.00	0.00
150	*180*	28	1.445	0.080	0.358	4.79E-06	0.05	0.05

the isolated case the RCC data shows a similar trend to WP85, despite small differences due to WP85 being a cuboid, not a cube. Different reference heights were used (10 m for WP85, 6 m for RCC), but assuming an "open terrain" 1/7 power wind profile this causes a ratio U_{6m}/U_{10m} of 0.93 which gives a small positive bias in U_{local}/U_{ref}. The WP85 U_{local} measurement was also done at the window itself, whereas the RCC local measurement is 3 m away from the window to avoid flow distortion, which could also lead to small positive bias.

Fig. 6a also shows the turbulence intensity (TI) measured at the local mast, σ_u/U_{local}, for each datapoint. TI values are much higher for $110° < \theta_{ref} < 180°$ and $\theta_{ref} < -150°$ when the mast is in the wake of both the test cube and the nearby storage shed. For flow approaching the front face of the cube ($-100° < \theta_{ref} < 100°$), TI lies between 0 and 0.5. For this site, the upstream wind profile has previously been measured by Ref. [36], giving an estimated roughness length $z_0 = 0.01$ m: assuming a neutral logarithmic wind profile, $U(z) = u_*/k\, ln\left(z/z_0\right)$, and a standard value of $\sigma_u/u_* = 2.5$ ([37]) gives an estimate for $\sigma_u/U \approx 0.2$. Crops were growing in the field during the isolated case which would have led to higher TI values due to a rougher surface than for previous campaigns.

For the array case, Fig. 6b shows much higher TI values due to wakes from surrounding buildings. The values are similar to previous studies

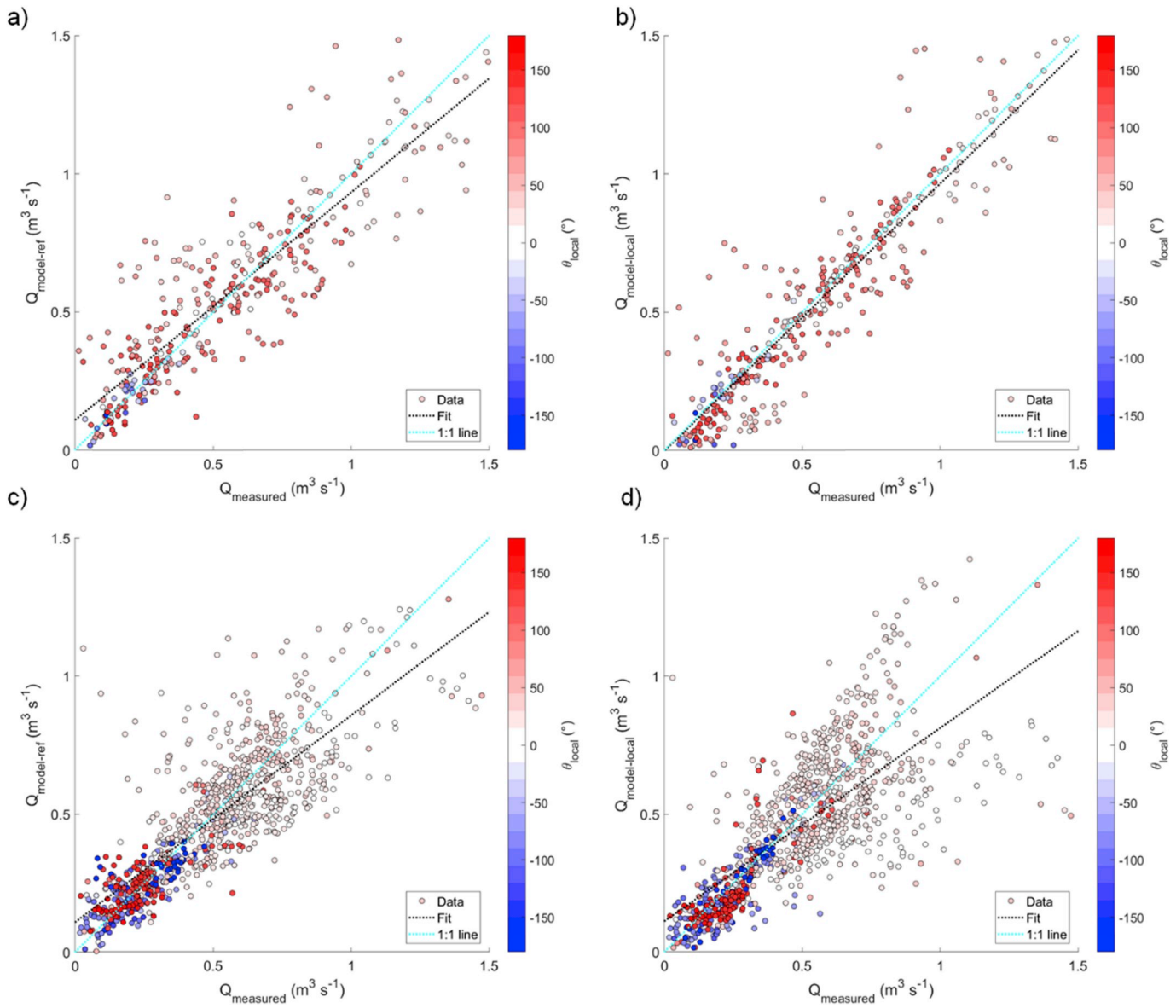

Fig. 5. Performance of WP85 ventilation rate model with RCC derived coefficients (Table 3-U_{ref} Table 4- U_{local}) for (a, b) isolated cube and (c, d) array case when (a, c) U_{ref} and θ_{local} and (b, d) U_{local} and θ_{local} are used. The 1:1 (cyan) line and a linear regression (black, Table 5) line are shown. Only sectors with (N > 5) are plotted as in Table 3 & Table 4. (For interpretation of the references to colour in this figure legend, the reader is referred to the Web version of this article.)

Table 5
Linear regression coefficients for model versus measured ventilation rate for the isolated and array cases for Fig. 5.

Case	Wind speed	N	Gradient	Offset	SE of Gradient	SE of offset	R^2	MAE	MBE
Isolated	U_{ref}	361	0.824	0.108	0.020	0.015	0.828	0.0580	0.0026
Isolated	U_{local}	361	0.967	−0.003	0.018	0.013	0.891	0.0228	−0.0023
Array	U_{ref}	908	0.749	0.109	0.018	0.010	0.664	0.0546	−0.01
Array	U_{local}	908	0.702	0.111	0.022	0.012	0.530	0.0685	−0.03

using arrays of cubes (TI = 0.3–5) ([38,39]) or measured around buildings in real urban areas (TI = 1–2) [40]. When TI > 1, this indicates that the flow influencing the ventilation at the opening is turbulence-dominated. Turbulence intensity in previous wind tunnel studies is much lower (i.e. < 5% [14], 10–20% [38]) and is not reported in other works, though is likely to be higher in the full-scale studies ([14–16]) due to surrounding buildings and trees.

5.3. Relating flow numbers to flow parameters

As the new coefficients (Section 5.1) for the RCC site are much larger than WP85 (C_{ref} = 0.025), it is hypothesised that turbulence is playing a role in increasing mean ventilation rate. This is reasonable as a) the RCC opening is relatively small and so unsteady ventilation processes can dominate [8] b) turbulence intensity is much larger than previous studies, and c) evidence in the literature shows that increased turbulence intensity leads to increased ventilation rate ([12,41]) and better agreement of simulations with experimental data [42].

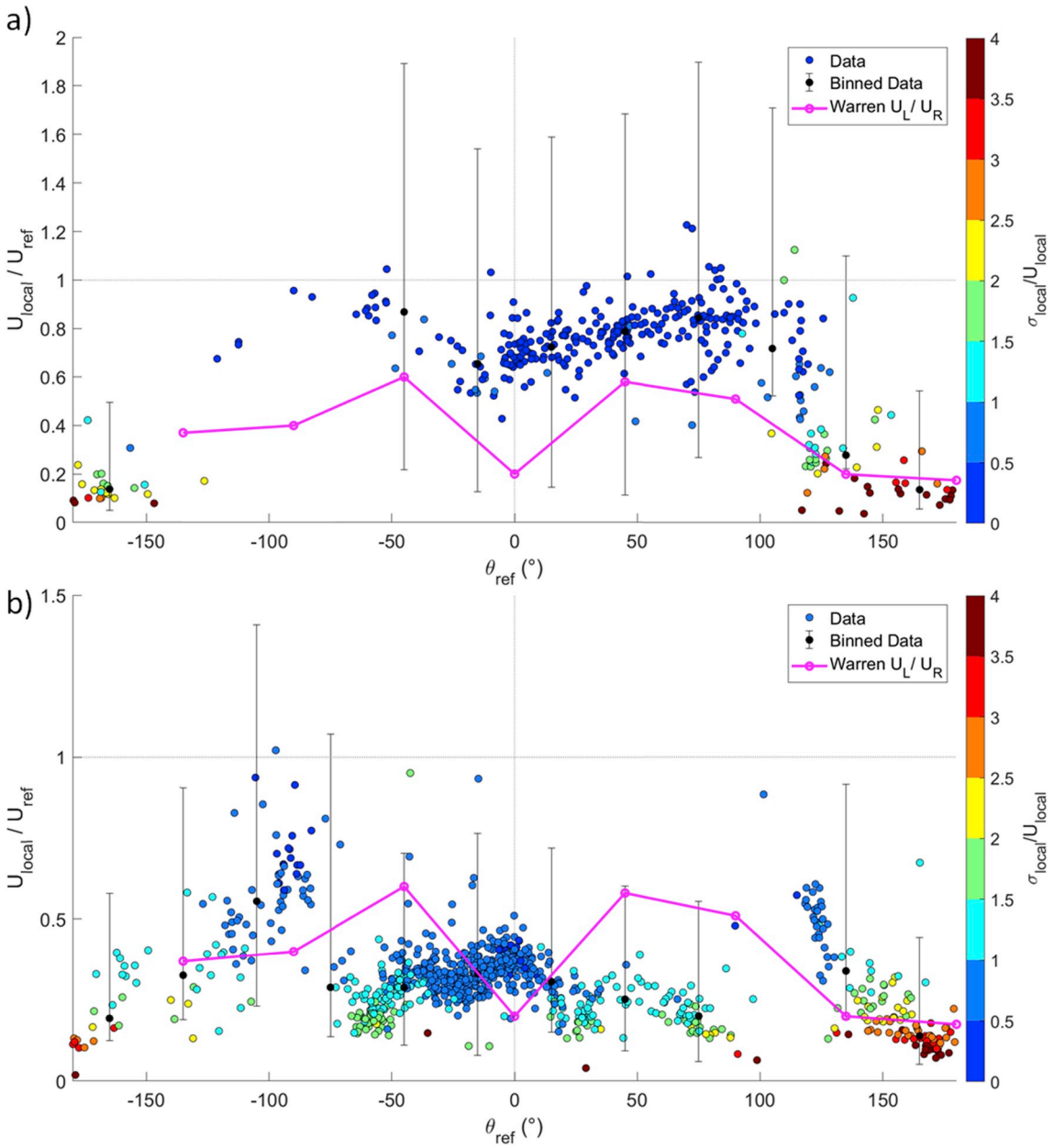

Fig. 6. Variation of the ratio of local to reference wind speed for all available RCC data with reference wind direction (θ_{ref}) for the a) isolated and b) array cases. Colour represents the turbulence intensity measured at the local mast (Fig. 1). Data is averaged into 30° bins and the median displayed if more than ten measurements are available. Error bars are the 5% and 95% bounds. Four outlying values of $U_{local}/U_{ref} \approx 4$ have been excluded. Data collected by WP85 and used by LH08 [14] shown as magenta solid line. (For interpretation of the references to colour in this figure legend, the reader is referred to the Web version of this article.)

For the isolated and array cases relations between flow number for all 30 min data-points (F_{ref}) and three dimensionless flow parameters are tested: U_{local}/U_{ref} (Fig. 7), local turbulence intensity σ_{local}/U_{local} (Fig. 8) and the product of the two $\frac{U_{local}}{U_{ref}} \frac{\sigma_{local}}{U_{local}}$ (Fig. 9). Linear regression coefficients are shown in Table 6. Data is split into windward (θ_{local} = -45°–45°) and leeward (θ_{local} = -135 to −180° and 135–180°) cases, as there is not enough data to cover the parallel case as in [14]. [14] notes that leeward flows are more likely to be dominated by unsteady forces than windward flow due to wake effects. This also suggests that for the array case, the windward flows will also be dominated by unsteady effects due to the wakes of the surrounding buildings.

Fig. 7a shows that for the isolated case, a linear relation between flow numbers and U_{local}/U_{ref} is found that is different for windward and leeward flows. Fig. 7b for the array case shows more scatter and an overlap of data-points for windward and leeward directions, demonstrating less directional dependence. There is a cluster of points (θ_{local} = −60° to −90°) which shows that even though local flow can be stronger, flow number is not necessarily higher.

Fig. 8a and b show no obvious linear relation between flow number and local turbulence intensity for both cases. For the isolated case a small number of points have $\sigma_{local}/U_{local} > 0.5$. In contrast for the array case most points have $\sigma_{local}/U_{local} > 0.5$ as wake flow dominates. It is notable that for leeward flow, there can be a wide range of σ_{local}/U_{local}, due to unsteady wake dynamics.

Fig. 9a shows that for the isolated case it is not clear that flow number variability is better explained by including σ_{local}/U_{local}. However, for the highly turbulent array case there is an improvement in the linear relation for the windward direction but not for leeward flows (Table 5). It is notable that the cluster with θ_{local} = −60° to −90° identified within Fig. 7b now sits within the other data-points, again

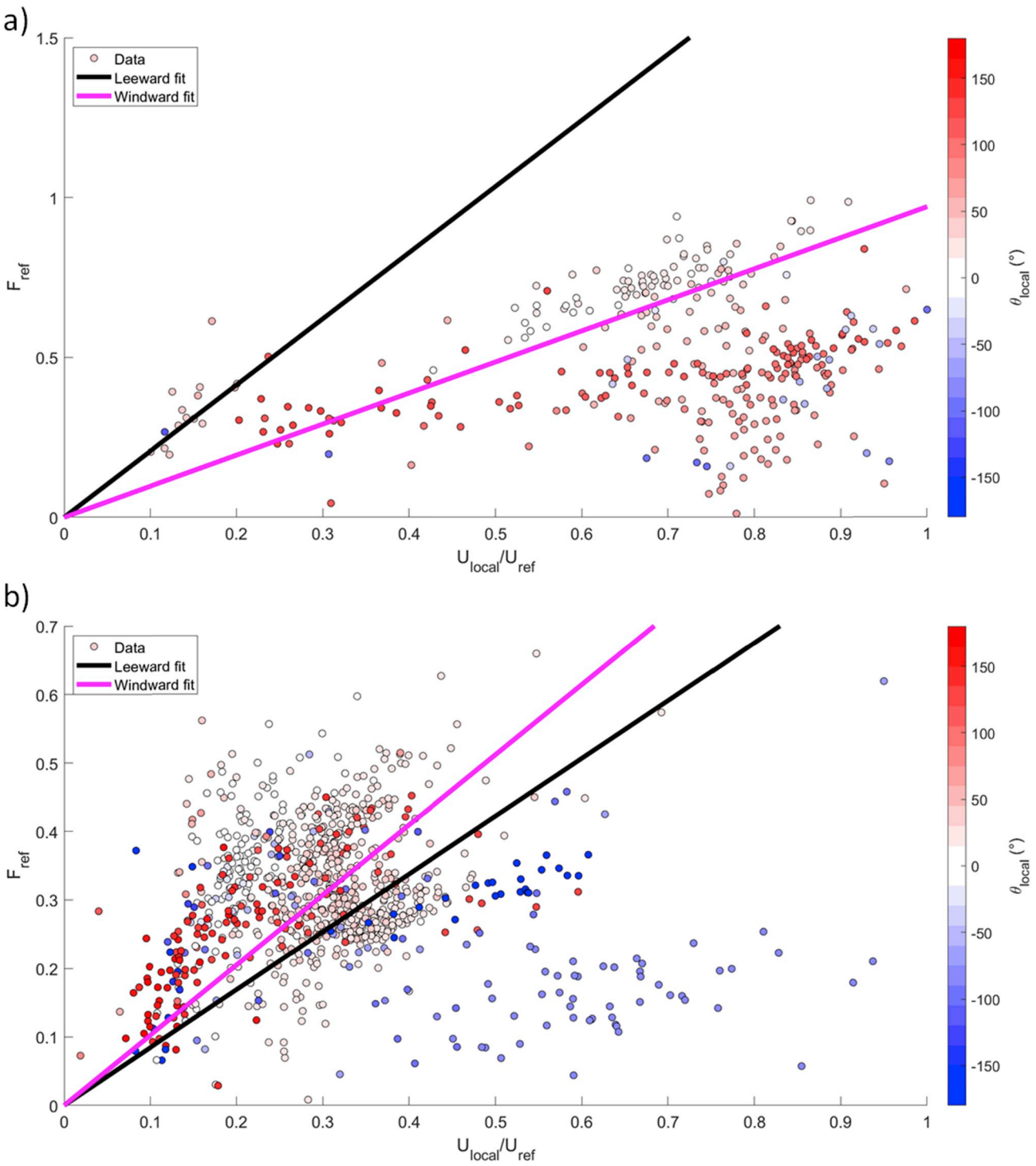

Fig. 7. Flow number F_{ref} dependence on $\frac{U_{local}}{U_{ref}}$ stratified by θ_{local} (colour) for a) isolated and b) array. Linear regression lines shown for windward (−45°–45°) and leeward (−135 to −180° and 135–180°) data. (For interpretation of the references to colour in this figure legend, the reader is referred to the Web version of this article.)

suggesting that ventilation rate could be better predicted by taking turbulence into account.

Overall this suggests that for highly turbulent flows in urban arrays ($\sigma_{local}/U_{local} > 0.5$), flow number is being enhanced by turbulence, and including it as a product with wind speed is appropriate. This form might provide an alternative to an additive term that [10] find to be problematic. The product term $\frac{U_{local}}{U_{ref}} \frac{\sigma_{local}}{U_{local}}$ equates to σ_{local}/U_{ref}, i.e. the amount of local turbulence produced for a given reference wind speed. The linear regressions shown in Fig. 9 give the relation:

$$F_{ref} = k \frac{U_{local}}{U_{ref}} . \frac{\sigma_{local}}{U_{local}} \quad (6)$$

which implies that the ventilation rate can be given by:

$$Q = kA\sigma_{local}. \quad (7)$$

This result may seem counter-intuitive as it does not include U_{ref}, but

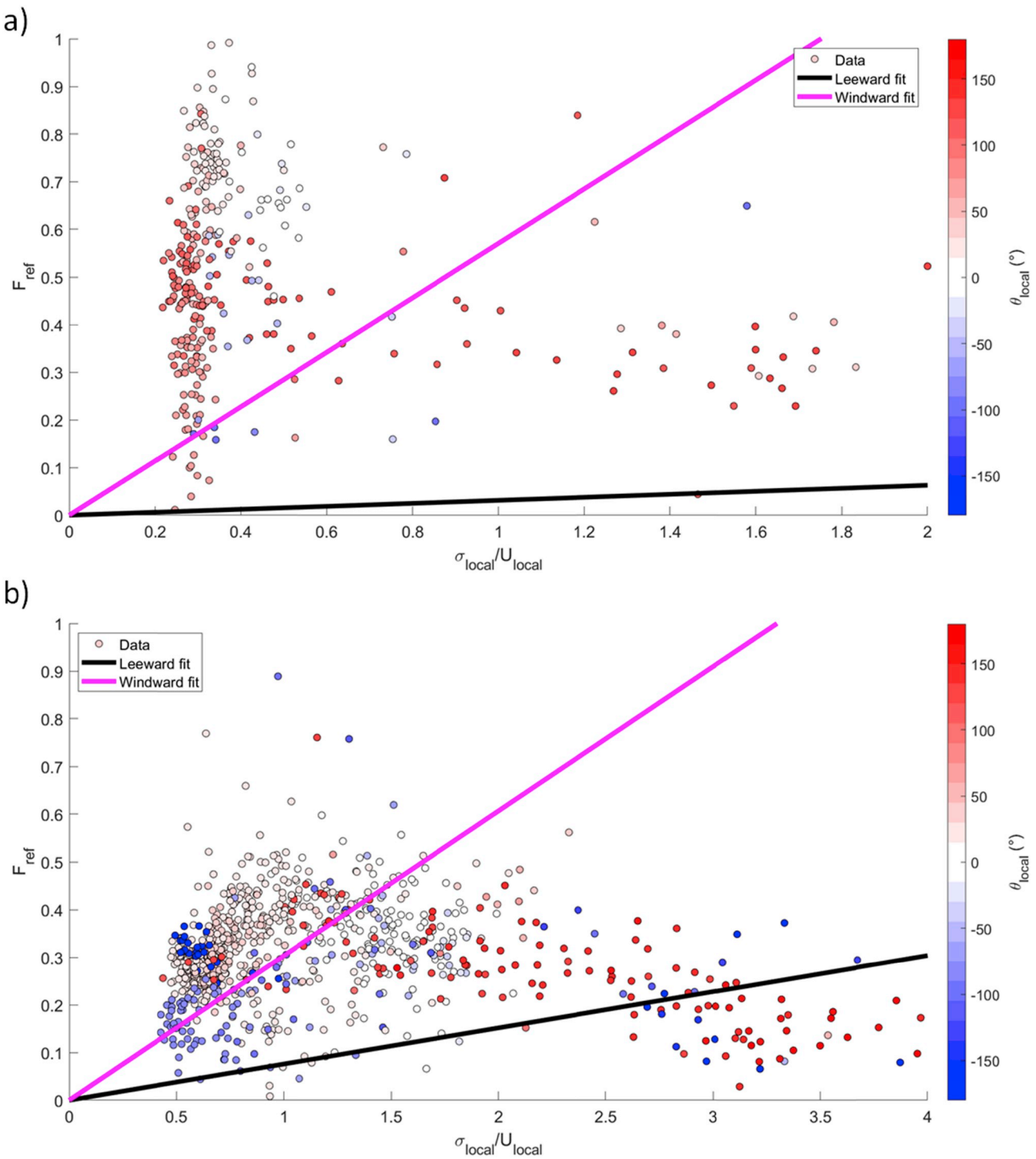

Fig. 8. As for Fig. 7, but with $\frac{\sigma_{local}}{U_{local}}$.

it should be borne in mind that in a wind-driven, neutral stability flow regime, turbulence increases in proportion to the driving flow, as turbulence intensity is constant.

5.4. Discussion

This analysis has presented evidence suggesting that the wind-driven model for single-sided ventilation in highly turbulent flows can be improved by including turbulence intensity as a factor. Elucidating the exact flow mechanism is for future model development studies, but it is worth recalling the main, unsteady mechanisms for wind-driven single-sided ventilation:

1) For flow parallel to the window, mixing layer or "eddy penetration". W77 derived a simple 2D mixing layer model for turbulence-free driving flow. In WP85, it was discussed that turbulence in the driving flow can thicken the mixing layer and thus enhance flow numbers. Indeed, WP85 results are based on full-scale measurements, and flow numbers are an order of magnitude larger than the W77 model, explained by both turbulence and "complex 3D flow effects". Given the present result that turbulence plays more of a role for the array case, this suggests there should be more focus on "non-

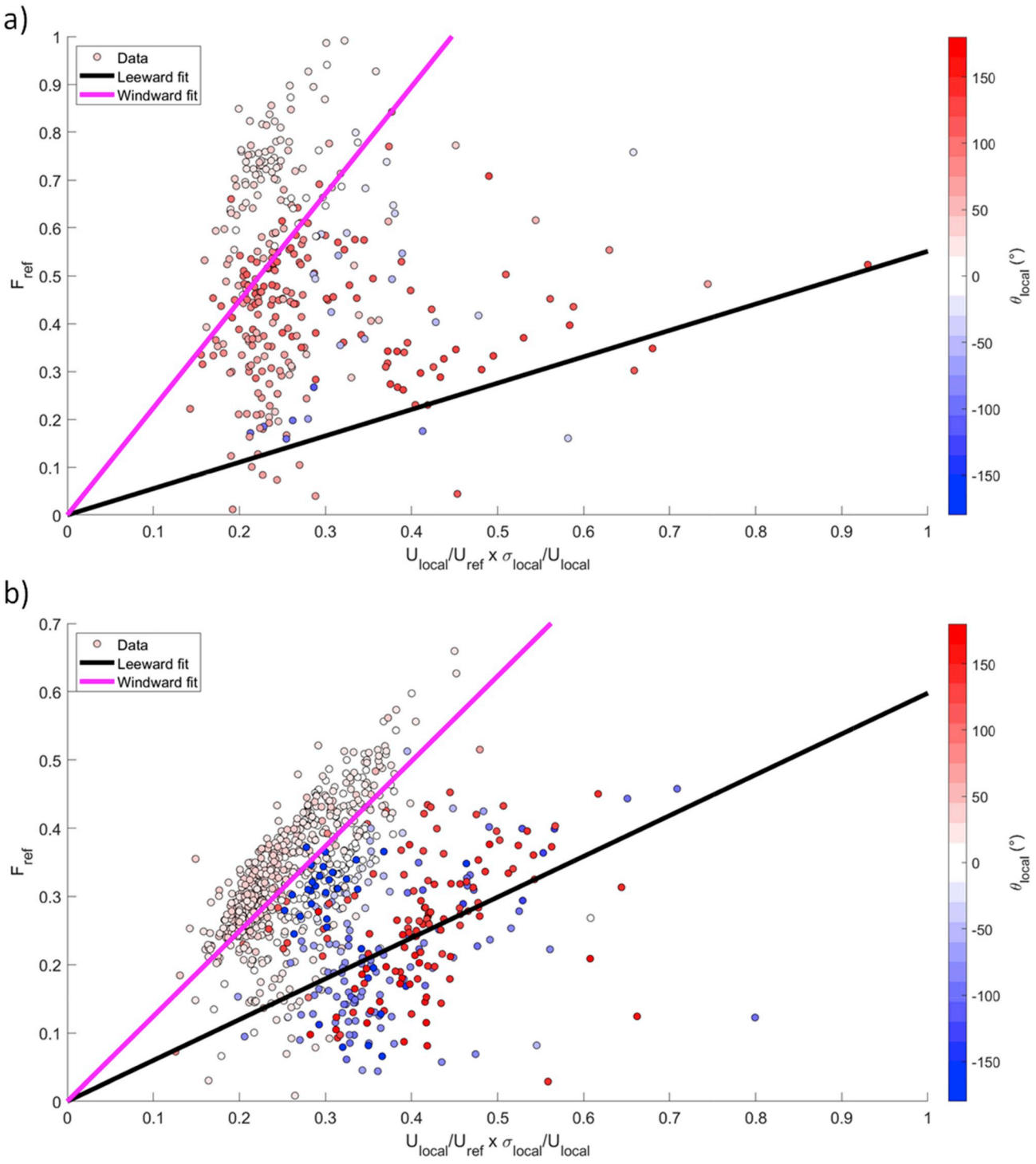

Fig. 9. As Fig. 7, but with $\left(\frac{U_{local}}{U_{ref}}\cdot\frac{\sigma_{local}}{U_{local}}\right)$.

2D" mixing layer processes and how mixing layer dynamics might be modified by larger eddies in the driving flow. An analogous area of work is ventilation from streets to the air above in the urban roughness sublayer (e.g. Fig 10. in [43]).

2) for perpendicular flow, the pulsation mechanism: longitudinal fluctuations in the perpendicular wind component cause pressure fluctuations due to the compressibility of air within the enclosure ([41, 44,45]). [41] undertook experiments to show that increasing turbulence intensity from 0.10 to 0.25 led to approximately 40% increase in flow number for their pulsation flow set-up. This suggests a sensitivity to turbulence in the driving flow which is distinct from the effect of having a small opening, which was highlighted in Section 2.

6. Conclusions

The novel, long-term, full-scale RCC dataset was used to test pre-existing models for single-sided ventilation rates for a simplified building (cube) with a small opening, both isolated and sheltered by an array of similar obstacles. The effect of sheltering on single sided ventilation rates has not been systematically tested previously due to a lack of local wind and turbulence measurements. The performance of previous

Table 6
Statistics of linear regressions for Figs. 7–9. The gradient, k, is defined in Equation (6).

	$\frac{U_{local}}{U_{ref}}$		$\frac{\sigma_{local}}{U_{local}}$		$\frac{U_{local}}{U_{ref}}\frac{\sigma_{local}}{U_{local}}$	
	Isolated windward	Isolated Leeward	Isolated windward	Isolated Leeward	Isolated windward	Isolated Leeward
N	124	9	124	9	124	9
k	0.971	2.069	0.571	0.031	2.238	0.551
SE k	0.020	0.293	0.069	0.011	0.087	0.039
R^2	0.615	0.654	0.406	0.385	0.326	0.671
p value	8.70E-82	0.000106	1.38E-13	0.024006	1.44E-51	5.87E-07
MAE	0.019	0.151	0.229	6.353	0.333	0.283
MBE	−0.019	0.151	−0.229	−6.353	0.333	−0.283
	Array Windward	Array Leeward	Array Windward	Array Leeward	Array Windward	Array Leeward
N	627	112	627	112	627	112
k	1.022	0.844	0.304	0.076	1.246	0.598
SE k	0.014	0.037	0.005	0.006	0.011	0.023
R^2	0.373	0.608	0.453	0.276	0.544	0.218
p value	3.89E-301	2.98E-43	7.04E-247	3.61E-22	0	9.68E-49
MAE	0.007	0.036	0.656	2.161	0.063	0.157
MBE	0.007	−0.036	−0.656	−2.161	0.063	−0.157

models is directly affected by variation in both wind speed and turbulence intensity with wind direction.

All models underestimated the ventilation rate of the cube, with the best performing model being Warren and Parkins (1985) [12] which agrees with the findings of [15]. Wind dominated over the stack effect for the RCC dataset. As results showed discrepancies that were directionally dependent, new coefficients were derived for the WP85 wind-driven model as a function of both local and reference wind speed and angle. Model predictions were improved most for the isolated case using the local wind speed. Predictions for the array case were generally improved using the local wind speed except for windward directions, perhaps due to the dual behaviour previously observed [23] (i.e. local measurement influenced by wake or channelled flow around buildings for the same reference wind direction.

Turbulence intensity local to the test building σ_{local}/U_{local} was mostly less than 0.5 for the isolated case but was between 0.5 and 4 for the sheltered case due to flow being wake-dominated. It was hypothesised that turbulence was enhancing ventilation, which could explain some of the underestimation by the models. To test this, flow number was related to U_{local}/U_{ref}, local turbulence intensity σ_{local}/U_{local} and the product of the two $\frac{U_{local}}{U_{ref}}\frac{\sigma_{local}}{U_{local}}$. There was no direct relation between flow number and turbulence intensity for both isolated and array cases. However, for the array case, the linear relation with $\frac{U_{local}}{U_{ref}}\frac{\sigma_{local}}{U_{local}}$ was better than for $\frac{U_{local}}{U_{ref}}$ alone. This suggests that in highly turbulent environments, turbulence does enhance mean ventilation rate to a degree [42]. Models could be improved by including a term which is multiplicative rather than additive as in LH08.

Conclusions drawn here are influenced by the specific set-up: the opening is small and of fixed size, internal volume large and flow is more turbulent and wind-driven than previous studies. Further testing is required for other configurations: different window sizes, shape and position, porosity, different building array layouts, conditions where the stack effect dominates. However, the case of small window openings with highly turbulent external flows is likely to be very common for buildings in densely urban areas. Previous models are based on data drawn from a narrow range of situations that do not represent all possible cases, in particular, sheltered urban buildings.

Declaration of competing interest

The authors declare that they have no known competing financial interests or personal relationships that could have appeared to influence the work reported in this paper.

Acknowledgements

This work was funded by the EPSRC and forms part of the REFRESH project, grant number: EP/K021893/1. Thanks to Solutions for Research and Roger Hoxey for assistance with the full-scale site. Datasets can be found at DOI: https://doi.org/10.17864/1947.137. The authors declare no conflict of interest.

References

[1] R. Ramponi, B. Blocken, CFD simulation of cross-ventilation for a generic isolated building: impact of computational parameters, Build. Environ. 53 (2012) 34–48, https://doi.org/10.1016/j.buildenv.2012.01.004.
[2] A. Tablada, F. De Troyer, B. Blocken, J. Carmeliet, H. Verschure, On natural ventilation and thermal comfort in compact urban environments–the Old Havana case, Build. Environ. 44 (2009) 1943–1958.
[3] G. Carrilho da Graça, P. Linden, Ten questions about natural ventilation of non-domestic buildings, Build. Environ. 107 (2016) 263–273, https://doi.org/10.1016/j.buildenv.2016.08.007.
[4] G.C. Da Graça, Q. Chen, L.R. Glicksman, L.K. Norford, Simulation of wind-driven ventilative cooling systems for an apartment building in Beijing and Shanghai, Energy Build. 34 (2002) 1–11.
[5] H. Wang, Q. Chen, A new empirical model for predicting single-sided, wind-driven natural ventilation in buildings, Energy Build. 54 (2012) 386–394, https://doi.org/10.1016/j.enbuild.2012.07.028.
[6] P.F. Linden, The fluid mechanics of Natural ventilation, Annu. Rev. Fluid Mech. 31 (1) (1999) 201–238.
[7] T. Peizhe, L. Liang, Z. Liguo, Z. Boyuan, Field measurement & research on natural ventilation performance of the new east-main building of China academy of building research (CABR), in: Procedia Eng, Elsevier, 2016, pp. 257–265, https://doi.org/10.1016/j.proeng.2016.06.385.
[8] J. Zhou, C. Ye, Y. Hu, H. Hemida, G. Zhang, W. Yang, Development of a model for single-sided, wind-driven natural ventilation in buildings, Build. Serv. Eng. Technol. 38 (2017) 381–399, https://doi.org/10.1177/0143624417699658.
[9] Y. Li, A. Delsante, Natural ventilation induced by combined wind and thermal forces, Build. Environ. 36 (2001) 59–71.
[10] T.S. Larsen, C. Plesner, V. Leprince, F.R. Carrié, A.K. Bejder, Calculation methods for single-sided natural ventilation: now and ahead, Energy Build. 177 (2018) 279–289, https://doi.org/10.1016/j.enbuild.2018.06.047.
[11] Q. Chen, Ventilation performance prediction for buildings: a method overview and recent applications, Build. Environ. 44 (2009) 848–858.
[12] P.R. Warren, L.M. Parkins, Single-sided ventilation through open windows, in: Conf. Proc. Therm. Perform. Exter. Envel. Build. ASHRAE, 1985, p. 20. Florida, http://www.scopus.com/inward/record.url?eid=2-s2.0-0021295517&partnerID=tZOtx3y1.
[13] P.R. Warren, Ventilation through openings on one wall only, Energy Conserv. Heat. Cool. Vent. Build. 1 (1977) 189–209. http://www.aivc.org/resource/ventilation-through-openings-one-wall-only. accessed March 15, 2016.
[14] T.S. Larsen, P. Heiselberg, Single-sided natural ventilation driven by wind pressure and temperature difference, Energy Build. 40 (2008) 1031–1040, https://doi.org/10.1016/j.enbuild.2006.07.012.
[15] M. Caciolo, P. Stabat, D. Marchio, Full scale experimental study of single-sided ventilation: analysis of stack and wind effects, Energy Build. 43 (2011) 1765–1773, https://doi.org/10.1016/j.enbuild.2011.03.019.
[16] M. Caciolo, S. Cui, P. Stabat, D. Marchio, Development of a new correlation for single-sided natural ventilation adapted to leeward conditions, Energy Build. 60 (2013) 372–382, https://doi.org/10.1016/j.enbuild.2013.01.024.

[17] W. De Gids, H. Phaff, Ventilation rates and energy consumption due to open windows: a brief overview of research in The Netherlands, Air Infiltration Rev. 4 (1982) 4–5.
[18] E. Dascalaki, M. Santamouris, A. Argiriou, C. Helmis, D.N. Asimakopoulos, K. Papadopoulos, A. Soilemes, On the combination of air velocity and flow measurements in single sided natural ventilation configurations, Energy Build. 24 (1996) 155–165.
[19] P. Stabat, M. Caciolo, D. Marchio, Progress on single-sided ventilation techniques for buildings, Adv. Build. Energy Res. 6 (2012) 212–241, https://doi.org/10.1080/17512549.2012.740903.
[20] CEN/TC 156, 16798-7:2017 Energy Performance of Buildings- Ventilation of Buildings - Part 7: Calculation Methods for the Determination of Air Flow Rates in Buildings Including Infiltration (Modules M5-5), 2017.
[21] H. Wang, Q. Chen, Modeling of the impact of different window types on single-sided natural ventilation, in: Energy Procedia, Elsevier, 2015, pp. 1549–1555, https://doi.org/10.1016/j.egypro.2015.11.201.
[22] H. Gough, Effects of Meteorological Conditions on Building Natural Ventilation in Idealised Urban Settings, PhD thesis, University of Reading, Department of Meteorology, 2017, http://centaur.reading.ac.uk/id/eprint/71951.
[23] H. Gough, T. Sato, C. Halios, C.S.B. Grimmond, Z. Luo, J.F. Barlow, A. Robertson, A. Hoxey, A. Quinn, Effects of variability of local winds on cross ventilation for a simplified building within a full-scale asymmetric array: overview of the Silsoe field campaign, J. Wind Eng. Ind. Aerodyn. 175C (2018) 408–418.
[24] H.L. Gough, Z. Luo, C.H. Halios, M.F. King, C.J. Noakes, C.S.B. Grimmond, J. F. Barlow, R. Hoxey, A.D. Quinn, Field measurement of natural ventilation rate in an idealised full-scale building located in a staggered urban array: comparison between tracer gas and pressure-based methods, Build. Environ. 137 (2018) 246–256, https://doi.org/10.1016/j.buildenv.2018.03.055.
[25] M.F. King, A. Khan, N. Delbosc, H.L. Gough, C. Halios, J.F. Barlow, C.J. Noakes, Modelling urban airflow and natural ventilation using a GPU-based lattice-Boltzmann method, Build. Environ. 125 (2017) 273–284, https://doi.org/10.1016/j.buildenv.2017.08.048.
[26] M.F. King, H.L. Gough, C. Halios, J.F. Barlow, A. Robertson, R. Hoxey, C.J. Noakes, Investigating the influence of neighbouring structures on natural ventilation potential of a full-scale cubical building using time-dependent CFD, J. Wind Eng. Ind. Aerodyn. 169 (2017) 265–279, https://doi.org/10.1016/j.jweia.2017.07.020.
[27] P.J. Richards, R.P. Hoxey, Unsteady flow on the sides of a 6m cube, J. Wind Eng. Ind. Aerodyn. 90 (2002) 1855–1866, https://doi.org/10.1016/S0167-6105(02)00293-3.
[28] P.J. Richards, R.P. Hoxey, Wind loads on the roof of a 6m cube, J. Wind Eng. Ind. Aerodyn. 96 (2008) 984–993, https://doi.org/10.1016/j.jweia.2007.06.032.
[29] J.F. Barlow, O. Coceal, A Review of Urban Roughness Sublayer Turbulence, 2009. http://research.metoffice.gov.uk/research/nwp/publications/papers/technical_reports/reports/527.pdf. (Accessed 20 May 2014).
[30] P.J. Richards, R.P. Hoxey, Pressures on a cubic building—Part 1: full-scale results, J. Wind Eng. Ind. Aerodyn. 102 (2012) 72–86, https://doi.org/10.1016/j.jweia.2011.11.004.
[31] P.J. Richards, R.P. Hoxey, Pressures on a cubic building-Part 2: quasi-steady and other processes, J. Wind Eng. Ind. Aerodyn. 102 (2012) 87–96, https://doi.org/10.1016/j.jweia.2011.11.003.
[32] M. Straw, C. Baker, A. Robertson, Experimental measurements and computations of the wind-induced ventilation of a cubic structure, J. Wind Eng. Ind. Aerodyn. 88 (2000) 213–230, https://doi.org/10.1016/S0167-6105(00)00050-7.
[33] M. Straw, Computation and Measurement of Wind Induced Ventilation, PhD thesis, University of Nottingham, 2000, http://etheses.nottingham.ac.uk/archive/00000110/. (Accessed 11 November 2013).
[34] N. Heijmans, P. Wouters, IEA Technical Report: impact of the uncertainties on wind pressures on the prediction of thermal comfort performances, Brussels, http://www.wtcb.be/homepage/download.cfm?dtype=europe&doc=TR23.pdf, 2002.
[35] A. Dobre, S.J. Arnold, R.J. Smalley, J.W.D. Boddy, J.F. Barlow, A.S. Tomlin, S. E. Belcher, Flow field measurements in the proximity of an urban intersection in London, UK, Atmos. Environ. 39 (2005) 4647–4657, https://doi.org/10.1016/j.atmosenv.2005.04.015.
[36] P. Richards, R. Hoxey, Unsteady flow on the sides of a 6m cube, J. Wind Eng. Ind. Aerodyn. 90 (2002) 1855–1866. http://www.sciencedirect.com/science/article/pii/S0167610502002933. (Accessed 11 November 2013).
[37] J.C. Kaimal, J.J. Finnigan, Atmospheric Boundary Layer Flows : Their Structure and Measurement: Their Structure and Measurement, Oxford University Press, 1993. http://books.google.com/books?id=ljbSonRztIcC&pgis=1. (Accessed 23 January 2014).
[38] J. Claus, O. Coceal, T.G. Thomas, S. Branford, S.E. Belcher, I.P. Castro, Wind-direction effects on urban-type flows, Boundary-Layer Meteorol. 142 (2011) 265–287, https://doi.org/10.1007/s10546-011-9667-4.
[39] H. Cheng, I.P. Castro, Near wall flow over urban-like roughness, Boundary-Layer Meteorol. 104 (2002) 229–259, https://doi.org/10.1023/A:1016060103448.
[40] A. Christen, Atmospheric turbulence and surface energy exchange in urban environments – results from the basel urban boundary layer experiment (BUBBLE), Stratus 11 (2005).
[41] J.P. Cockroft, P. Robertson, Ventilation of an enclosure through a single opening, Build. Environ. 11 (1976) 29–35, https://doi.org/10.1016/0360-1323(76)90016-0.
[42] Y. Jiang, D. Alexander, H. Jenkins, R. Arthur, Q. Chen, Natural ventilation in buildings: measurement in a wind tunnel and numerical simulation with large-eddy simulation, J. Wind Eng. Ind. Aerodyn. 91 (2003) 331–353, https://doi.org/10.1016/S0167-6105(02)00380-X.
[43] O. Coceal, A. Dobre, T. Thomas, Unsteady dynamics and organized structures from DNS over an idealized building canopy, Int. J. 1953 (2007) 1943–1953, https://doi.org/10.1002/joc.
[44] F. Haghighat, J. Rao, P. Fazio, The influence of turbulent wind on air change rates—a modelling approach, Build. Environ. 26 (1991) 95–109, https://doi.org/10.1016/0360-1323(91)90017-6.
[45] J. Zhou, D. Fan, Y. Hu, G. Zhang, W. Yang, Calculation of single-sided ventilation due to unsteady wind pressure Part 1 pulsating rate, in: Proc. 13th Int. Conf. Indoor Air Qual. Clim, 2014, pp. 538–545.